Latitudinal Variations of the Convective Source and Propagation Condition of Inertio-Gravity Waves in the Tropics

HYE-YEONG CHUN, JUNG-SUK GOH, AND IN-SUN SONG

Department of Atmospheric Sciences, Yonsei University, Seoul, South Korea

LUCREZIA RICCIARDULLI

Remote Sensing Systems, Santa Rosa, California

(Manuscript received 21 October 2005, in final form 25 May 2006)

ABSTRACT

Latitudinal variations of the convective source and vertical propagation condition of inertio-gravity waves (IGWs) in the tropical region (30°S–30°N) are examined using high-resolution Global Cloud Imagery (GCI) and 6-hourly NCEP–NCAR reanalysis data, respectively, for 1 yr (March 1985–February 1986). The convective source is estimated by calculating the deep convective heating (DCH) rate using the brightness temperature of the GCI data. The latitudinal variation of DCH is found to be significant throughout the year. The ratio of the maximum to minimum values of DCH in the annual mean is 3.2 and it is much larger in the June–August (JJA) and December–February (DJF) means. Spectral analyses show that DCH has a dominant period of 1 day, a zonal wavelength of about 1600 km, and a Gaussian-type phase-speed spectrum with a peak at the zero phase speed.

The vertical propagation condition of IGWs is determined, in the zonal wavenumber and frequency domain, by two factors: (i) latitude, which determines the Coriolis parameter, and (ii) the basic-state wind structure in the target height range of wave propagation. It was found that the basic-state wind significantly influences the wave propagation condition in the lower stratosphere between 150 and 30 hPa, and accordingly a large portion of the source spectrum is filtered out. This is prominent not only in the latitudes higher than 15° where strong negative shear exists, but also near the equator where strong positive shear associated with the westerly phase of the quasi-biennial oscillation (QBO) filters out large portions of the low-frequency components of the convective source. There is no simple relationship between the ground-based frequency and latitude; lower latitudes are not always favorable for low-frequency IGWs to be observed in the stratosphere. The basic-state wind in the Tropics, which has seasonal, annual, and interannual variations, plays a major role not only in determining the wave propagation condition in the stratosphere but also in producing convective sources in the troposphere.

1. Introduction

During the last decade, convectively forced gravity waves have received a great deal of attention from both observational and numerical modeling groups. Convectively forced gravity waves that have a wide phase-speed spectrum can propagate up to the mesosphere without seasonal restriction and contribute significantly to the momentum budget in the middle atmosphere. Observational evidence of convective gravity waves has been reported from radiosondes (e.g., Allen and Vincent 1995; Karoly et al. 1996; Vincent and Alexander 2000; Tsuda et al. 2004), rocket soundings (e.g., Eckermann et al. 1995), and satellite measurements (e.g., Fetzer and Gille 1994; Wu and Waters 1996; McLandress et al. 2000; Tsuda et al. 2000; Ern et al. 2004; Jiang et al. 2004). Compared with the first two measurements, which are conducted at a limited number of geographical locations, global distribution of gravity wave variances is available from the satellite measurements. Even though satellite-derived gravity wave variance or momentum flux for each preceding study is somewhat limited in its own observational restrictions on horizontal and vertical wavelengths and frequency, strong peaks of wave energy or momentum flux appear in the

Corresponding author address: Prof. Hye-Yeong Chun, Department of Atmospheric Sciences, Yonsei University, Shinchon-dong, Seodaemun-ku, Seoul 120-749, South Korea.
E-mail: chy@atmos.yonsei.ac.kr

DOI: 10.1175/JAS3891.1

tropical latitudes. Strong positive correlation between gravity wave variance and outgoing longwave radiation or cloudiness in summertime has been shown in most of the aforementioned studies, which suggests the importance of cumulus convection as a source of atmospheric gravity waves that are observed in the stratosphere.

Recently, Alexander et al. (2002) suggested a different interpretation of the observed peaks of gravity waves with short vertical wavelengths in the low latitudes, based on the dispersion relationship of inertio–gravity waves. They showed that the intrinsic frequency of vertically propagating inertio-gravity waves can be smaller in the lower latitudes due to the smaller value of the Coriolis parameter. Consequently, the vertical component of group velocity can be smaller in the lower latitudes, since it decreases as the intrinsic frequency decreases. With these two factors, they suggested that there is more chance for such low-frequency waves to be observed in the lower latitudes, because the maximum period of gravity waves becomes longer there and the waves stay longer in the stratosphere before they propagate out from the observational altitudes. Based on a simple ray-tracing model, Bühler (2003) also suggested that the spectral peak of potential energy at the equator is due to equatorward propagation of inertio-gravity waves that are generated by convective sources even in strictly extratropical regions. This result can be equally valid for poleward propagation of inertio-gravity waves that are induced by equatorial wave sources.

Even though Alexander et al. (2002) and Bühler (2003) have nicely demonstrated the importance of latitudinal preference of wave propagation in the interpretation of gravity wave activity observed from radiosondes and satellite measurements, (i) they do not take into account latitudinal distribution of wave sources and (ii) their arguments are all based on intrinsic frequency, which may not be useful for direct comparison with ground-based observations. Wave source and wave propagation condition are the two major factors that determine the properties of gravity waves. Based on high-resolution numerical simulations of two-dimensional squall lines, which explicitly calculate convective gravity waves in the stratosphere, Song et al. (2003) showed that the characteristics of gravity waves are determined by the spectral combination of wave sources and wave propagation condition. The spectral combination of the wave source and wave propagation condition is included explicitly in the formulation of momentum flux spectrum of convectively forced gravity wave drag (GWD) parameterizations that have been developed recently by Beres et al. (2004), Beres (2004), and Song and Chun (2005). Therefore, it is more realistic to take into account wave propagation condition (relative to the ground) and wave source together in interpreting the latitudinal distribution of the observed wave variances.

In this study, we derive the convective wave source in the tropical region between 30°S and 30°N based on the deep convective heating rate proposed by Ricciardulli and Garcia (2000) using Global Cloud Imagery (GCI) data for 1 yr (March 1985–February 1986). The vertical propagation condition of the inertio-gravity waves (IGWs) is calculated using the National Centers for Environmental Prediction–National Center for Atmospheric Research (NCEP–NCAR) reanalysis data (Kalnay et al. 1996). The spectral combination of wave source and wave propagation condition as a function of latitude presented here can lead to a more complete understanding of latitudinal variations of the observed gravity waves at low latitudes, presumably generated by convective sources. In section 2, we present data and methodology to calculate the convective source. Latitudinal and seasonal variations of the convective source, and power spectral density of the convective source in the zonal wavenumber and frequency domain also are presented. In section 3, we calculate the propagation condition of IGWs and present the spectral combination of the wave source and wave propagation condition. Summary and conclusions are given in the last section.

2. Convective source

The convective source derived in the present study is the deep convective heating (DCH) rate defined by Ricciardulli and Garcia (2000) using mean brightness temperature (TBR) derived from the GCI data. GCI is a high-resolution dataset, with a horizontal resolution of 0.35° in latitude and 0.7° in longitude at every 3 h, that has been created by Tanaka et al. (1991) and Salby et al. (1991) based on the International Satellite Cloud Climatology Project (ISCCP) data. The GCI data are chosen in the present study mainly due to their high spatial and temporal resolutions, which allow a wide range of zonal wavenumber and frequency spectra. Several studies have been done using the GCI data (i) to investigate equatorial waves (planetary and gravity waves) generated by convective heating that is projected onto Hough modes (e.g., Bergman and Salby 1994; Ricciardulli and Garcia 2000), (ii) to understand the local and space scales of organized tropical convection for use in validation of convective processes in current global circulation models (e.g., Ricciardulli and Sardeshmukh 2002), and (iii) to understand the role of deep convective clouds in the tropical region in maintaining temperature and humidity near the tropical tropopause (e.g., Salby et al. 2003).

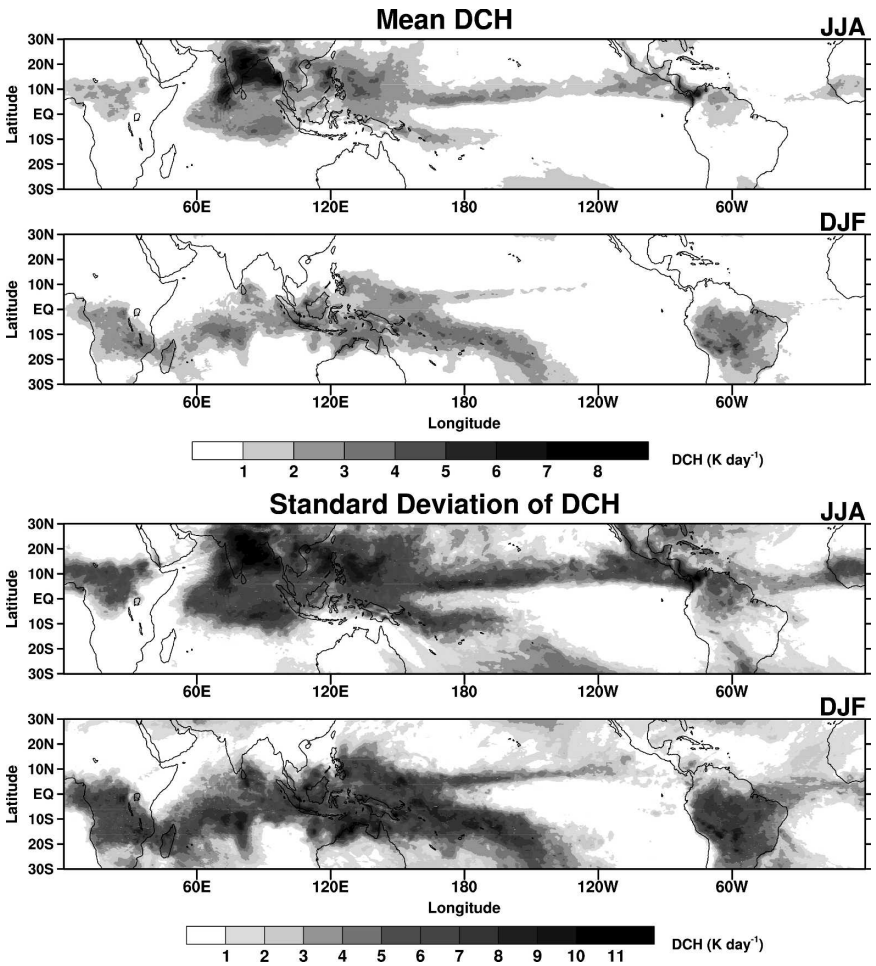

FIG. 1. Global distribution of the DCH in the tropical region between 30°S and 30°N calculated using the GCI data and (1), averaged over JJA 1985 and DJF 1985/86 and their standard deviations.

Following Ricciardulli and Garcia (2000), DCH can be converted from a deep convective activity (DCA) index by

$$\mathrm{DCH} = \alpha_c \, \mathrm{DCA}, \tag{1}$$

where

$$\mathrm{DCA} = \begin{cases} 240\ \mathrm{K} - \mathrm{TBR} & \text{if} \quad \mathrm{TBR} < 240\ \mathrm{K} \\ 0 & \text{otherwise.} \end{cases} \tag{2}$$

Here, α_c is a converting parameter, which can be derived based on the relationships between the observed precipitation and DCH and between the observed precipitation and DCA, and TBR is the brightness temperature of the cloud. The detailed derivations can be found in Ricciardulli and Garcia (2000), but in the present study we briefly describe the procedure to derive (1). The latent heating rate by condensation of water vapor, which is represented by DCH, is proportional to precipitation amount, $J/c_p = 0.24P$, where J/c_p (K day^{-1}) is the heating rate and P (mm day^{-1}) is the precipitation rate. In this calculation, a vertically uniform heating with a depth of 10.3 km is assumed. The relationship between the precipitation and DCA index is obtained by comparing the observed mean precipitation in the tropical region (21°N–21°S) during the years 1986–89 by Janowiak and Arkin (1991; 4 mm day^{-1}) to the mean DCA during March 1985–February 1986 for which the present study is considered (1.32 DCA units). This provides $P = 3.0$ DCA. Then, using the relationship between the DCH and P, we can obtain (1) with $\alpha_c = 0.73$. Considering that the period of the present DCA dataset is not directly matched to that of the precipitation dataset of Janowiak and Arkin (1991), the above conversion may not be accurate. However, since the seasonal and interannual deviations from the 1986–89 mean precipitation are shown to be within 10% of

the mean value by Janowiak and Arkin (1991), this problem may not be severe, as pointed out by Ricciardulli and Garcia (2000). It is noteworthy, however, that the magnitude of DCA (and DCH) depends directly on the choice of a threshold brightness temperature [240 K in (1)] that represents the "deep" convection criterion in the tropical region. As discussed by Ricciardulli and Sardeshmukh (2002), the threshold brightness temperature of 240 K represents reasonably well the deep convective clouds that should be distinguished from the high cold cirrus clouds.

Figure 1 shows the global distribution of DCH averaged over June–August (JJA) 1985 and December 1985–February 1986 (DJF) and their standard deviations. In the present study, the JJA and DJF means are considered rather than the annual mean (except in Fig. 2), since the latitudinal distribution of the convective source in the tropical region varies according to the seasonal change of the intertropical convergence zone (ITCZ). In JJA, strong convective activity occurs in the Indian continent and nearby ocean with a secondary maximum near Mexico, while in DJF the convective sources exist mainly in western Pacific and South America. The maximum magnitude of DCH is larger (8.19 K day^{-1}) in JJA than in DJF (5.98 K day^{-1}). The standard deviation of DCH is much larger than the mean value, even though its global distribution is similar to the mean distribution, and its magnitude in DJF is comparable to that in JJA. The large value of the standard deviation is mainly due to the high-frequency component with a period shorter than 2 days (not shown). The result in DJF is similar to that by Ricciardulli and Garcia (2000), covering the period of 14 November 1983–20 March 1984 with $\alpha_c = 0.87$.

Figure 2 shows the latitudinal distribution of DCH in JJA, DJF, and annual means. The annual mean is calculated using the monthly averaged DCH. There exists a strong latitudinal variation of convective source in the tropical region between 30°S and 30°N. The maximum heating rate exists at 9.7°N with a value of 2.1 K day^{-1} in JJA, while it is at 8.3°S with a value of 1.7 K day^{-1} in DJF. This seasonal difference in the latitudinal distribution of DCH produces a smoother annual mean distribution with a primary peak at 7.2°N, 1.5 K day^{-1} and a secondary peak at 5.4°S, 1.3 K day^{-1}. Sharp changes of DCH with respect to latitude are shown in all three means, and the gradient of the DCH within just 5° latitude is significant. This is most prominent in JJA, and DCH at 5°N (1.5 K day^{-1}) is reduced by about half at the equator (to 0.8 K day^{-1}). The ratio of the maximum to minimum (23.4°S, 0.4 K day^{-1}) values of DCH in the annual mean is 3.8, while those in JJA and DJF are much larger (22.5 and 20.3, respectively). These values

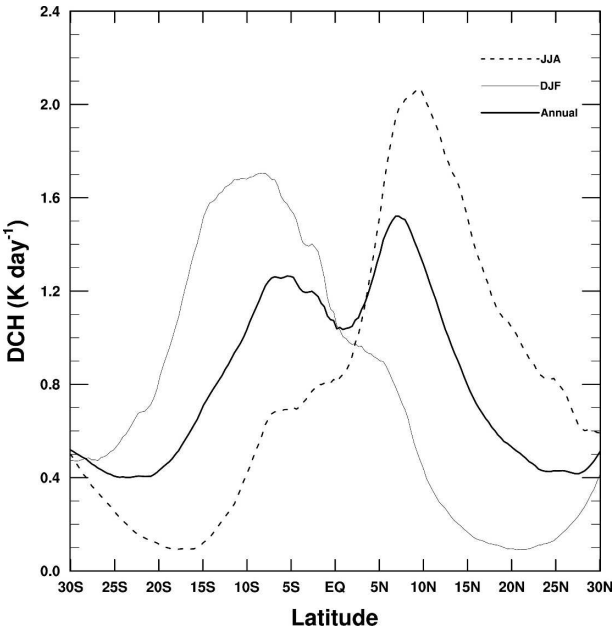

FIG. 2. Latitudinal distribution of zonally averaged DCH in the JJA (dotted line), DJF (thin line), and annual (thick line) means over March 1985–February 1986.

are at least twice larger than the ratio of low-latitude (5°) to high-latitude (35°) wave potential energy (1.9) averaged over all seasons of satellite observation by Tsuda et al. (2000), which has been the primary observational evidence to explain the importance of the wave propagation condition and to suggest a spectral slope for gravity wave drag parameterization (Alexander et al. 2002). The ratio of low-latitude (5°N) to high-latitude (30°N) DCH in the present annual mean is 2.7, which is still much larger than the ratio of the aforementioned wave energy. This implies that the latitudinal variation of convective sources should be considered in the interpretation of the latitudinal variation of observed gravity waves, which was neglected in Alexander et al. (2002).

Figure 3 shows the power spectral density (PSD) of DCH with respect to frequency (ω) as a function of latitude for JJA and DJF (Fig. 3a) and its latitudinal average in an area-preserving form (Fig. 3b). To obtain PSD with respect to frequency, a two-dimensional spectrum of DCH with respect to frequency and zonal wavenumber is calculated at each latitude circle using a two-dimensional fast Fourier transform (FFT). Then, the two-dimensional power spectrum is integrated over zonal wavenumber at each latitudinal circle. The positive (negative) frequency denotes an eastward (westward) moving component of DCH. The frequency spectrum of DCH shows several interesting features. First, westward- and eastward-moving components of

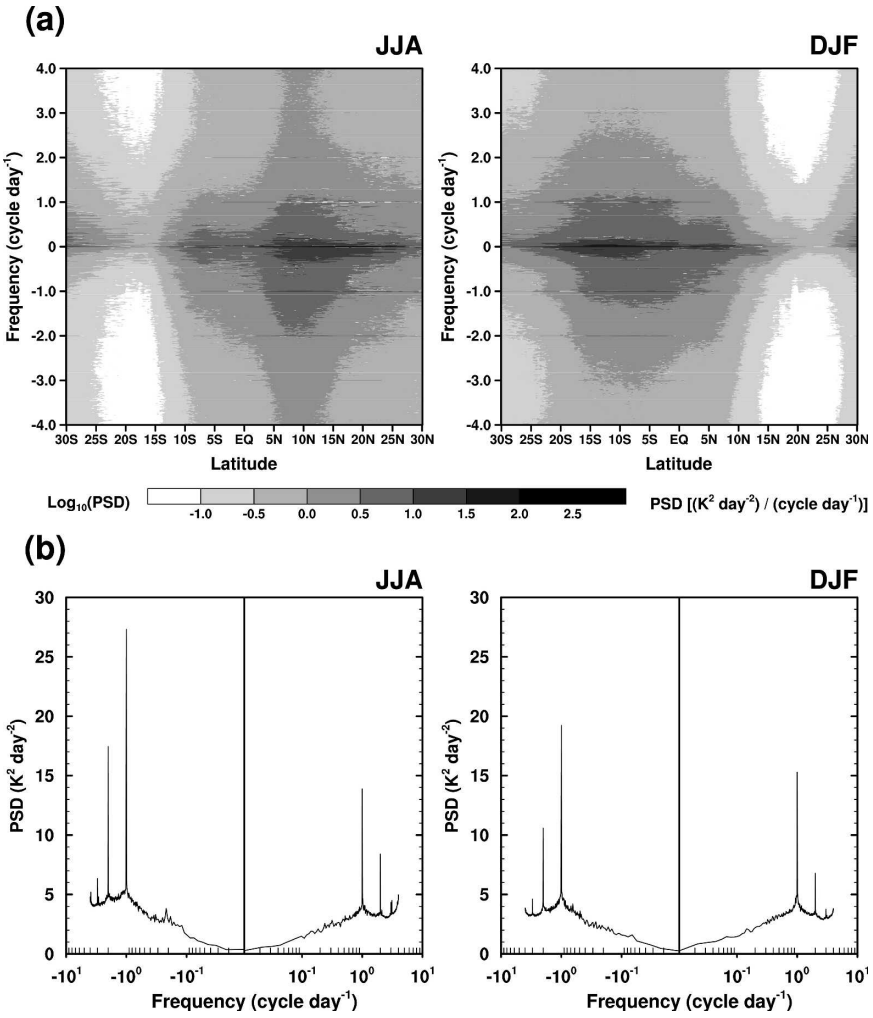

FIG. 3. (a) Latitude–frequency cross section of the PSD of DCH and (b) latitudinally averaged PSD with respect to frequency in an area preserving form for (left) JJA and (right) DJF.

the convective source are nearly symmetric in all latitudes with respect to the stationary component, although the westward-moving component has a slightly stronger power, especially in JJA. Strong convective activities occur in 10°S–30°N for JJA and 10°N–30°S for DJF, according to the seasonal change of ITCZ, while the minimum PSD appears near 15°–20°S in JJA and 15°–25°N in DJF. Second, the stationary component of the convective source has a maximum PSD, and components with periods longer than 24 h $< \pm 1.0$ cpd have relatively large PSDs in the major convective region. The component with a 12 h-period (2 cpd) is also noticeable in the major forcing region. In the area-preserving form of PSD averaged over all latitudes (Fig. 3b), a primary spectral peak appears at 24 h and a secondary peak at 12 h for both JJA and DJF, which is consistent with the previous studies using the GCI data (Bergman and Salby 1994; Ricciardulli and Garcia 2000; Ricciardulli and Sardeshmukh 2002).

Figure 4 shows the PSD of DCH with respect to zonal wavenumber (k) as a function of latitude for JJA and DJF (Fig. 4a) and its latitudinal average in an area-preserving form (Fig. 4b). For calculating PSD with respect to zonal wavenumber, the two-dimensional spectrum of DCH, which was previously calculated in Fig. 3, is integrated over frequency at each latitudinal circle. In all latitudes, PSD is maximal at small wavenumbers (long wavelengths) and it decreases as the wavenumber increases. In the major forcing region (ITCZ), zonal wavelengths longer than about 800 km are dominant in both JJA and DJF. In JJA, the region for large PSDs at a given zonal wavenumber is relatively localized (5°–15°N) compared with that in DJF (0°–15°S) due to the sharp decrease of DCH from 5°N to the equator in JJA,

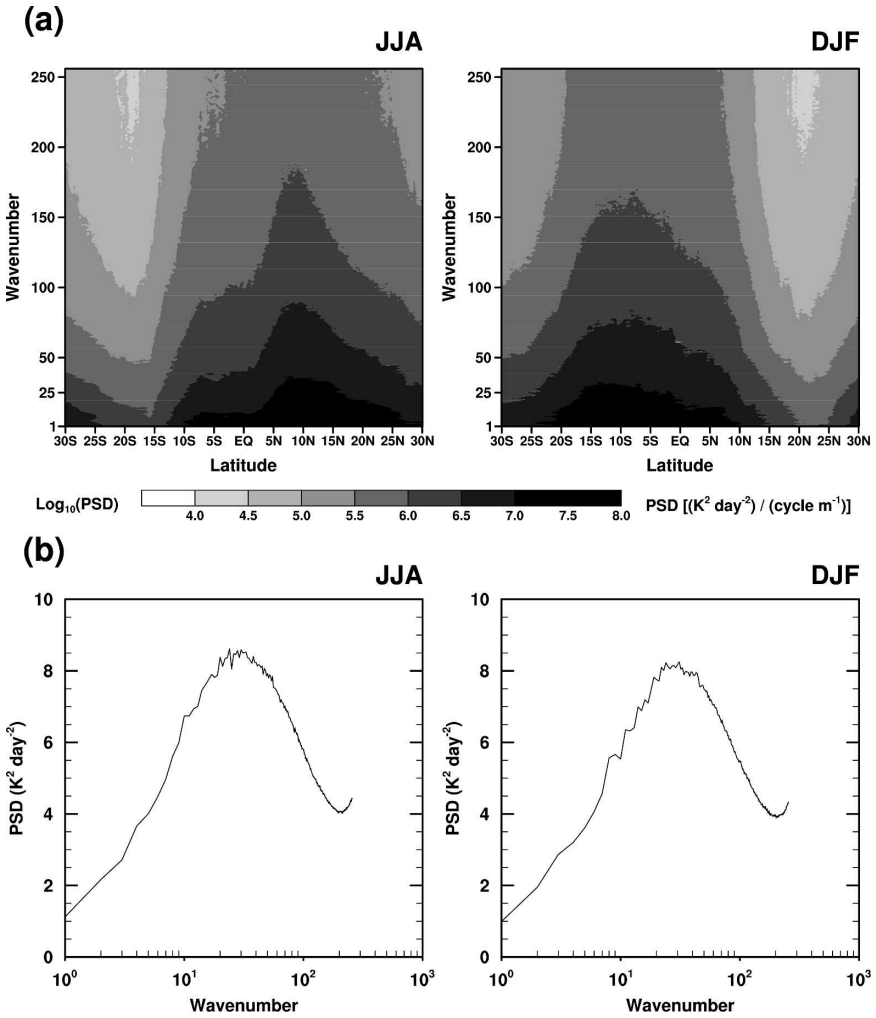

FIG. 4. Same as in Fig. 3, but for the zonal wavenumber.

as mentioned earlier in Fig. 2. Latitudinally averaged PSD (Fig. 4b) indicates that the dominant power is at zonal wavenumbers ranging from 15 to 60 in JJA and from 20 to 50 in DJF with a spectral peak at $k = 24$, in both JJA and DJF, which corresponds to a zonal wavelength of about 1600 km. It is important to note that this value is almost one order of magnitude larger than the spatial scale of DCA given by Ricciardulli and Sardeshmukh (2002), which ranges from 95 to 115 km over continents and from 110 km to 170 km over the oceans, which is defined as a distance at which the spatial lag autocorrelation of DCA falls to 1/e. This difference may be because the zonal wavelength calculated from a spectral analysis represents global (nonlocal) information on convection, while the spatial scale by Ricciardulli and Sardeshmukh (2002) represents local features of organized convection.

Figure 5 shows the PSD of DCH with respect to phase speed for JJA and DJF (Fig. 5a) and its latitudinal average (Fig. 5b). To obtain the phase speed, the two-dimensional spectrum of DCH with respect to frequency and zonal wavenumber, which was previously calculated in Fig. 3, is used. The phase-speed spectrum is calculated using 2 m s^{-1} phase-speed bins. The spectral power at each bin c_o represents the integration of the two-dimensional PSD with respect to k and ω over the area where $c_o - 1.0 < \omega/k < c_o + 1.0$. A detailed description of the phase-speed calculation can be found in Song et al. (2003). The PSD of DCH is maximal for the stationary component at all latitudes, and it deceases sharply as the phase speed increases. The eastward- and westward-moving components of DCH are nearly symmetric with respect to the stationary phase, but the westward-moving component has a slightly larger spectral power in the major forcing region in JJA.

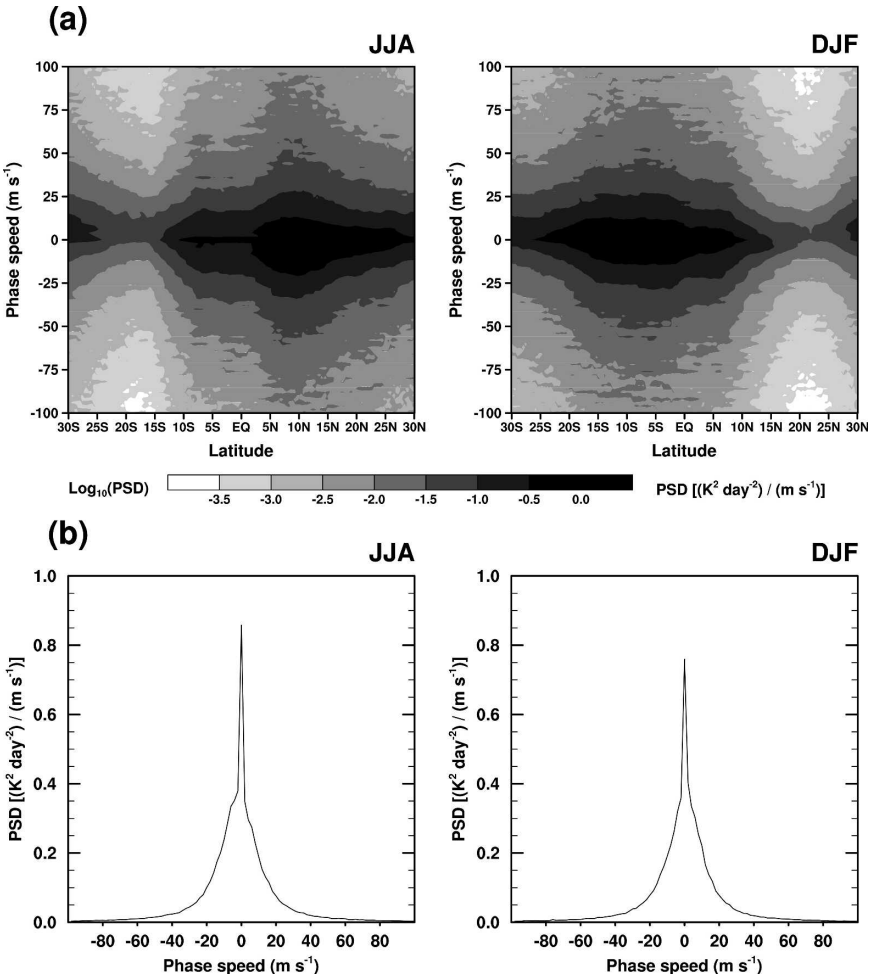

FIG. 5. Same as in Fig. 3, but for the zonal phase speed.

The latitudinally averaged phase-speed spectrum of DCH shown in Fig. 5b is similar to the diabatic-forcing spectrum used in the convective GWD parameterizations that have been developed recently by Beres et al. (2004) and Song and Chun (2005, hereafter SC05), which is calculated based on a Gaussian-type forcing in zonal direction and time [Eqs. (23)–(24) of SC05]. Furthermore, the spectral shape of DCH is nearly the same in all latitudes between 30°S and 30°N and each season, although the magnitude of PSD varies latitudinally, as shown in Fig. 5a. This implies that the diabatic forcing specified in the aforementioned convective GWD parameterizations represents reasonably well the convective heating estimated by DCH in the tropical region. Given that the diabatic-forcing spectrum is a crucial factor in determining the reference-level momentum flux spectrum, the forcing spectrum used in the convective GWD parameterizations needs a certain degree of reality. The GCI data, with their relatively high temporal and spatial resolutions, are invaluable resources to estimate the spectral structure of convective forcing that is directly useful for validation of convective GWD parameterization, and to estimate the temporal and spatial scales as well as global distribution of convection, which cannot be well represented in current GCMs.

It may be necessary to estimate the spectral structure of convective forcing in the extratropical regions, which is not covered with the present GCI data, and to validate the Gaussian-type forcing used in the aforementioned convective GWD parameterization. However, given that the magnitudes of reference-level momentum flux and resultant wave drag as well as convective forcing are predominant in the tropical region between 30°S and 30°N, as shown in Chun et al. (2004), the influence of the forcing spectrum in the convective GWD parameterization in the extratropical regions is not likely to be significant. There are, however, exceptional latitudes associated with storm tracks in the winter hemisphere (30°–40°N in January and 30°–40°S in

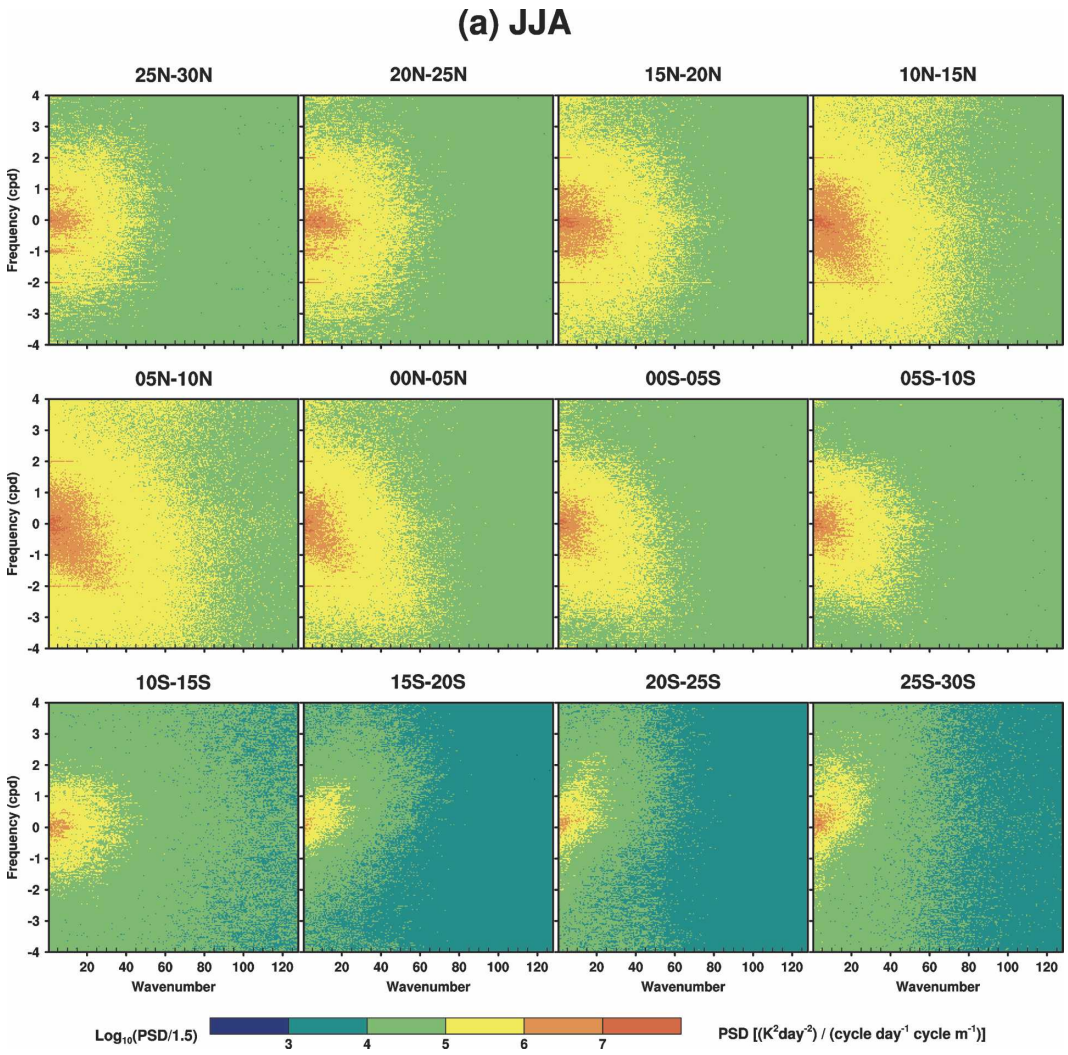

FIG. 6. Wavenumber–frequency cross section of the PSD of DCH in each 5° latitude bin calculated for the (a) JJA and (b) DJF periods.

July) at which the magnitude of cloud-top momentum flux is not negligibly small compared with that in tropical regions (Song 2005), and observational studies to characterize convective sources in those regions may be necessary.

Figure 6 shows the PSD of DCH in the zonal wavenumber and frequency domain for each 5° latitude bin for JJA and DJF. Since latitudinal variation of DCH is significant as shown in Fig. 2, we calculate the PSD of DCH averaged over a rather fine latitude bin. In JJA (Fig. 6a), strong convective activity occurs in the latitudes between 0° and 20°N. The maximum PSD exists at the stationary component, and relatively large PSD exists at the period larger than 1 day. The 24-h (1 cpd) component has a large PSD for all latitudes, and the 12-h (2 cpd) component shows relatively large PSD for the latitudes between 5° and 30°N but exclusively for zonal wavenumbers less than 20 (equivalent zonal wavelengths larger than 1740–2000 km). Especially in major forcing regions (5°–15°N), a relatively large PSD exists for high-frequency components that have periods between 6 and 12 h. In this major forcing region, relatively large PSD extends to large (short) zonal wavenumbers (wavelengths) of 60–80 (500–650 km). Especially, DCH (with near-zero frequency and zonal wavenumbers larger than about 60) has a strong power exclusively in 0°–20°S in DJF, and, as will be shown in Fig. 9b, gravity waves generated by this source spectrum in 5°–15°S can propagate up to the middle atmosphere, which may contribute significantly to the large-scale circulation. Except in this strong forcing region, DCH with zonal wavelengths larger than about 1000 km

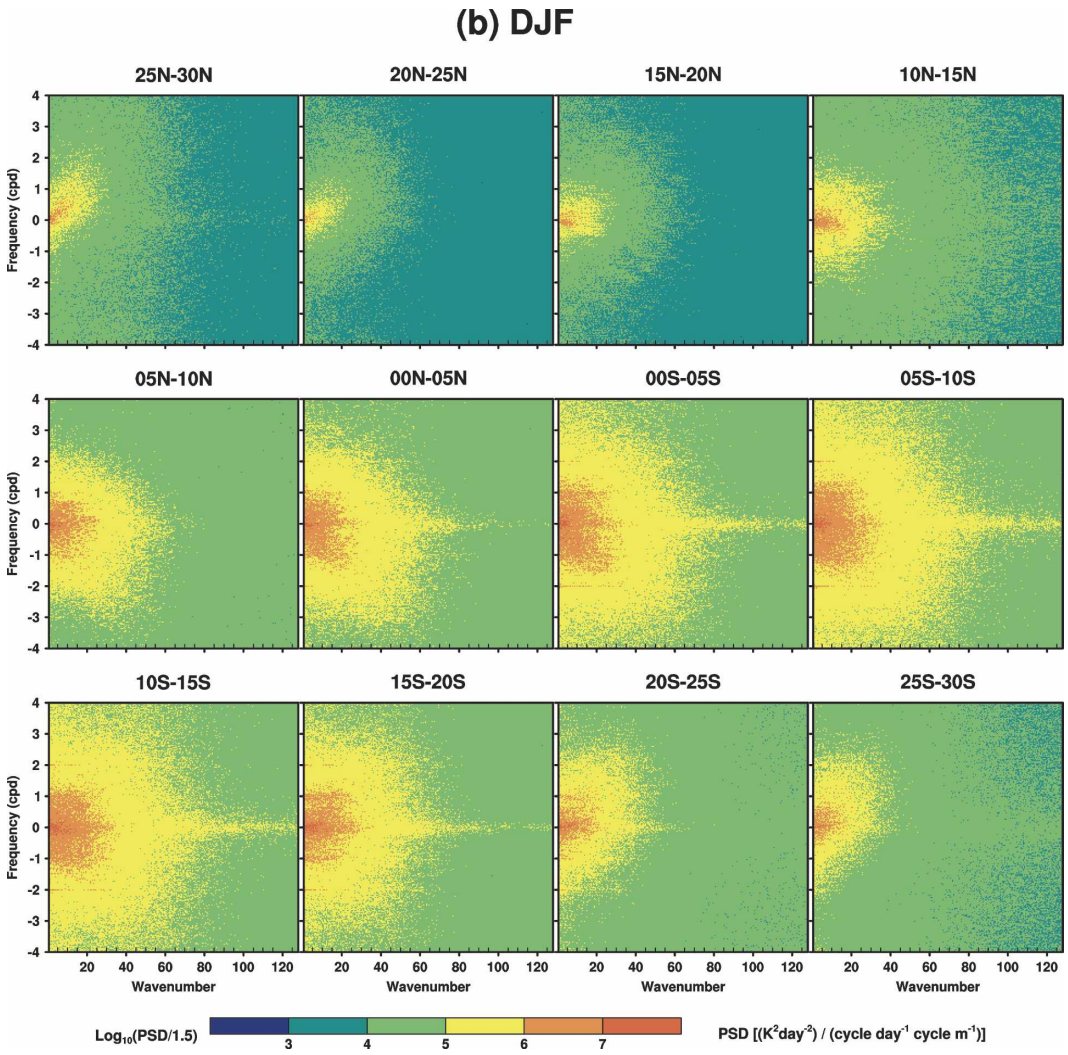

FIG. 6. (*Continued*)

is dominant. The westward-moving component of the convective source dominates the eastward-moving component for 15°N–10°S. The opposite is true south of 15°S, while the components are almost symmetric north of 15°N. In DJF (Fig. 6b), the spectral distribution of DCH is somewhat different from that in JJA. First, the westward- and eastward-moving components of DCH are nearly symmetric, except north of 20°N and south of 25°S where the eastward-moving components are dominant. This is why the phase-speed spectrum in DJF (right panel of Fig. 5b) is more symmetric than in JJA. Second, in the major forcing region (0°–20°S), the relatively large PSD for the near-stationary component extends to very large zonal wavenumbers. This is why the PSDs at large zonal wavenumbers lie in a wider latitudinal region of ITCZ in DJF than in JJA, as shown in Fig. 4a.

It is noteworthy that the forcing spectrum shown in Fig. 6 is not all used to generate gravity waves that can propagate up to the stratosphere. This is because the characteristics of gravity waves are determined by the spectral combination of the wave source and the wave propagation condition, and the forcing to generate gravity waves propagating into the stratosphere is the *effective forcing* that is filtered by the wave propagation condition in the spectral domain (Song et al. 2003). To understand the characteristics of gravity waves in the stratosphere, therefore, one should consider the wave source and the wave propagation condition together in their spectral domain.

3. Wave propagation condition

The dispersion relation of the three-dimensional IGWs can be written as (Marks and Eckermann 1995)

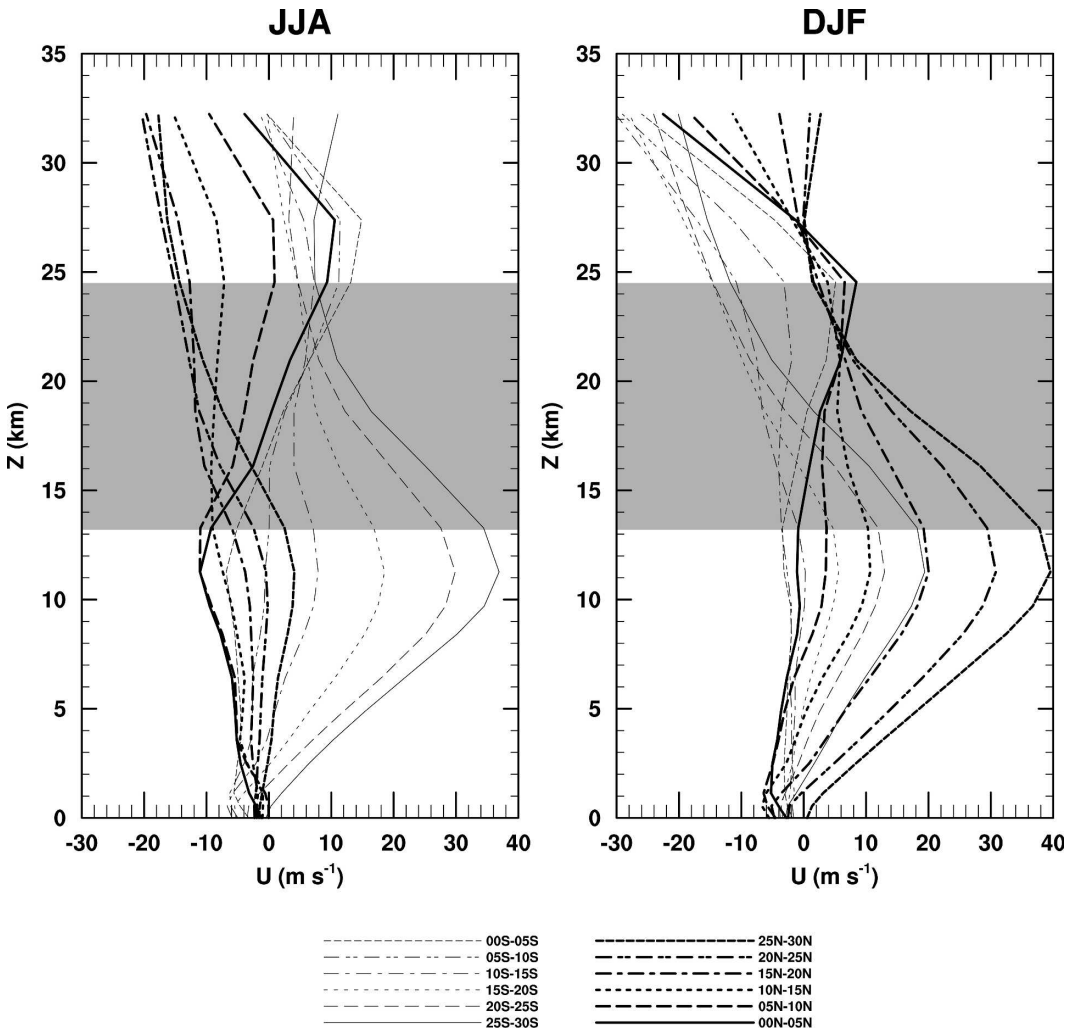

FIG. 7. Vertical profiles of the zonal-mean zonal wind averaged over each 5° latitude bin and three months in JJA and DJF calculated using the NCEP–NCAR reanalysis data.

$$\hat{\omega} = (\omega - Uk - Vl)^2 = \frac{N^2(k^2 + l^2) + f^2(m^2 + \alpha^2)}{k^2 + l^2 + m^2 + \alpha^2}. \tag{3}$$

Here, $\hat{\omega}$ is the intrinsic frequency; ω is the ground-relative frequency; k, l, and m are the zonal, meridional, and vertical components of the wavenumber, respectively; U and V are the zonal and meridional components of the basic-state wind, respectively; N is the Brunt–Väisälä frequency; f is the Coriolis parameter; and $\alpha = 1/4H_\rho^2$, where H_ρ is the density scale height. Equation (3) can be rewritten as

$$m^2 = \frac{(\hat{\omega}_c^2 - \hat{\omega}^2)(k^2 + l^2 + \alpha^2)}{\hat{\omega}^2 - f^2}, \tag{4}$$

where

$$\hat{\omega}_c^2 = N^2 - \frac{\alpha^2(N^2 - f^2)}{k^2 + l^2 + \alpha^2}. \tag{5}$$

Here, $\hat{\omega}_c$ is the high-frequency cutoff for waves of a given horizontal wavenumber $(k^2 + l^2)^{1/2}$, which can be derived by setting $m = 0$. From (4), the vertical propagation condition of IGWs ($m^2 > 0$) is

$$f^2 < \hat{\omega}^2 (\equiv \omega - Uk - Vl)^2 < \hat{\omega}_c^2 \leq N^2. \tag{6}$$

Note that if the vertical gradient of the basic-state density is neglected ($\alpha^2 = 0$), $\hat{\omega}_c$ equals to N, and, as will be shown later, including α merely leads to filtering out some high-frequency components of IGWs with very small zonal wavenumbers.

The propagation condition of gravity waves from 150

to 30 hPa is calculated at each 5° latitude bin by neglecting meridional propagation ($l = 0$), using (6) and zonal-mean zonal wind and temperature calculated using the 6-hourly NCEP–NCAR reanalysis data. The NCEP–NCAR data have a horizontal grid spacing of 2.5° latitude × 2.5° longitude and 17 vertical levels from the surface to 10 hPa. The 150 and 30 hPa were chosen, respectively, as a top of convective source in the tropical region and a middle stratosphere height at which most radiosonde and some satellite measurement analyses have been conducted (e.g., Allen and Vincent 1995; McLandress et al. 2000; Ern et al. 2004; Jiang et al. 2004).

Figure 7 shows the JJA and DJF means of the zonal-mean zonal wind profiles averaged over each 5° latitude bin used for calculation of wave propagation condition. (The Brunt–Väisälä frequency profiles are not shown because their latitudinal variation is negligibly small.) Latitudinal variation of the zonal-mean zonal wind is significant in both the troposphere and stratosphere. Strong positive shear exists in the winter hemisphere below $z = 11$ km between 15° and 30° and for the latitude bin of 25°–30°S in DJF. DCH at these latitudes is significantly smaller than at the other latitudes. This proves that strong shear in the troposphere prevents development of deep convective clouds by blowing out the clouds from their original location before they become tall. In the target height range of 150–30 hPa (i.e., an equivalent geometric height range of 13.2–24.5 km), relatively strong positive shears exist in the low latitudes between 10°S and 10°N in both JJA and DJF where major convective activity occurred, while negative shears occur in the most of remaining regions. The vertical propagation condition of IGWs relative to the ground in (6) varies not only by latitude through the monotonic change of the Coriolis parameter, but also by the basic-state wind that changes in latitude in a nonmonotonic manner. Thus, it is not straightforward to confirm that low-frequency waves are more easily observed in lower than higher latitudes, simply because the Coriolis parameter is smaller in lower latitudes. Since wave properties and wave sources are observed relative to the ground, rather than following the motion, background wind should be included in wave propagation arguments.

In the zonal wavenumber–frequency domain, the vertical propagation condition of IGWs can be determined by the basic-state wind and stability through the dispersion relation in (6) at a given latitude. For convenience, we denote with k_p and ω_p the zonal wavenumber and frequency that prohibit vertical propagation of IGW. Since the upper limit of (6) is satisfied mostly in the k–ω domain that ranges based on the temporal and spatial resolutions of the present DCH data, the area of $k_p - \omega_p$ is determined mainly by the condition to violate the lower limit of (6). There exists a negligibly small $k_p - \omega_p$area to violate the upper limit of (6) in very high frequency and very small wavenumber regions, which is due to including the vertical variation of basic-state air density (α).

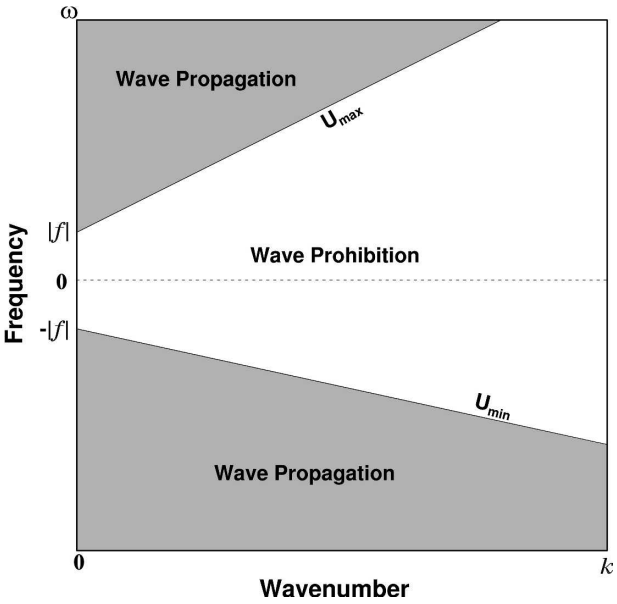

FIG. 8. A schematic diagram to represent the vertical propagation condition of IGWs given by (7)–(8) in a zonal wavenumber–frequency domain, when a basic-state wind changes from $U_{\min}$ and $U_{\max}$ in a target height range of wave propagation.

It is straightforward to show that the lower limit of (6) $[f^2 < (\omega - Uk)^2]$ is equivalent to

$$\omega > Uk + |f| \quad \text{for} \quad \omega - Uk > 0, \tag{7}$$

$$\omega < Uk - |f| \quad \text{and} \quad \omega - Uk < 0, \tag{8}$$

in both hemispheres. This implies that the area of $k_p - \omega$ is enclosed by two zonal phase speeds (slope in the $k-\omega$ domain) that are equal to the minimum and maximum of the basic-state wind in a target height range with the intercepts of $\omega = -|f|$ and $\omega = +|f|$, respectively. A schematic diagram illustrating (7) and (8) for a given basic-state wind profile in a target height range, which changes from the minimum ($U_{\min}$) to maximum ($U_{\max}$) is shown in Fig. 8. It is clear from Fig. 8 that the propagation condition of low-frequency IGWs is determined by two factors: the basic-state wind (and wind shear), and the latitude at which the magnitude of intercept ($\omega = |f|$) is determined. For a given basic-state wind profile, low-frequency waves are easy to propagate upward (i.e., less $k_p - \omega_p$ area) in lower latitudes than in higher latitudes due to smaller value of the

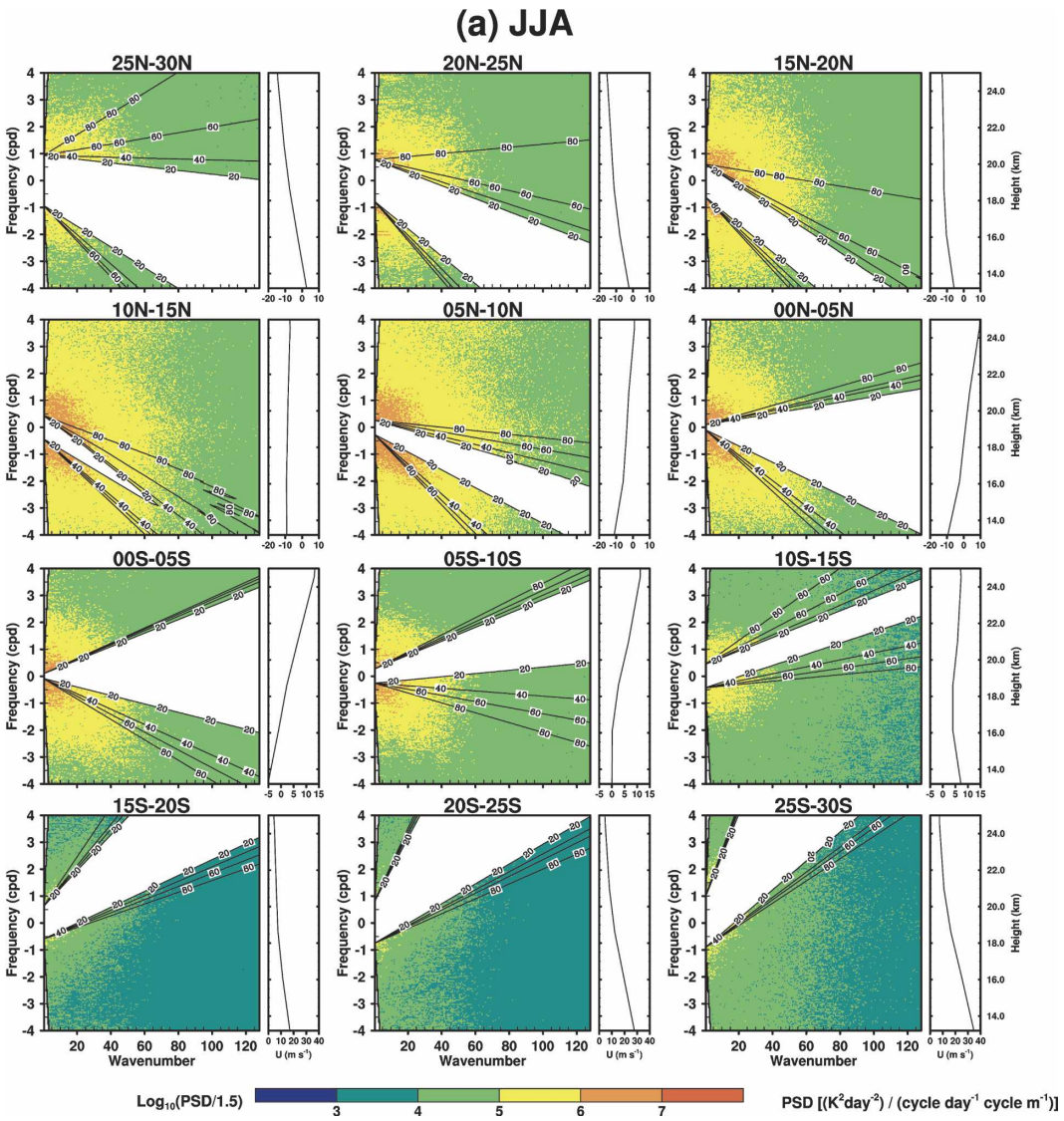

FIG. 9. Percentage (lines with numbers) of which certain spectral region satisfies vertical propagation of IGWs during the 3-month periods of (a) JJA and (b) DJF, superimposed on the PSD of DCH shown in Fig. 6. Above the upper percentage line and below the lower percentage line denote the area for wave propagation with that percentage. The white area denotes the spectral domain that allows less than 20% of wave propagation during the 3-month period.

intercept. However, this cannot be guaranteed when the basic-state wind shear is stronger in lower latitudes. Note that the wind shear in the lower stratosphere, as shown in Fig. 7, is quite large in the lower latitudes, especially in JJA near the equator, which changes from a weak easterly in the troposphere to a relatively strong westerly in the stratosphere. Considering that the stratospheric zonal-mean zonal wind near the equator is strongly related to the quasi-biennial oscillation (QBO), the zonal-mean zonal wind will be changed based on the evolution of QBO. Strong positive shear in the lower stratosphere occurs in the present westerly QBO phase, and consequently, large portions of the positive phase-speed components of wave spectrum will be filtered out in the lower stratosphere.

Figure 9 shows a spectral domain that satisfies the vertical propagation condition of IGWs during the JJA (Fig. 9a) and DJF (Fig. 9b) periods superimposed on the PSD of DCH as shown in Fig. 6. The wave propagation condition is calculated based on (6) by using the 6-hourly NCEP–NCAR reanalysis data in the target height range (150–30 hPa). Except for a negligibly small area with very small zonal wavenumber and high frequency that violates the upper limit of (6), the spectral

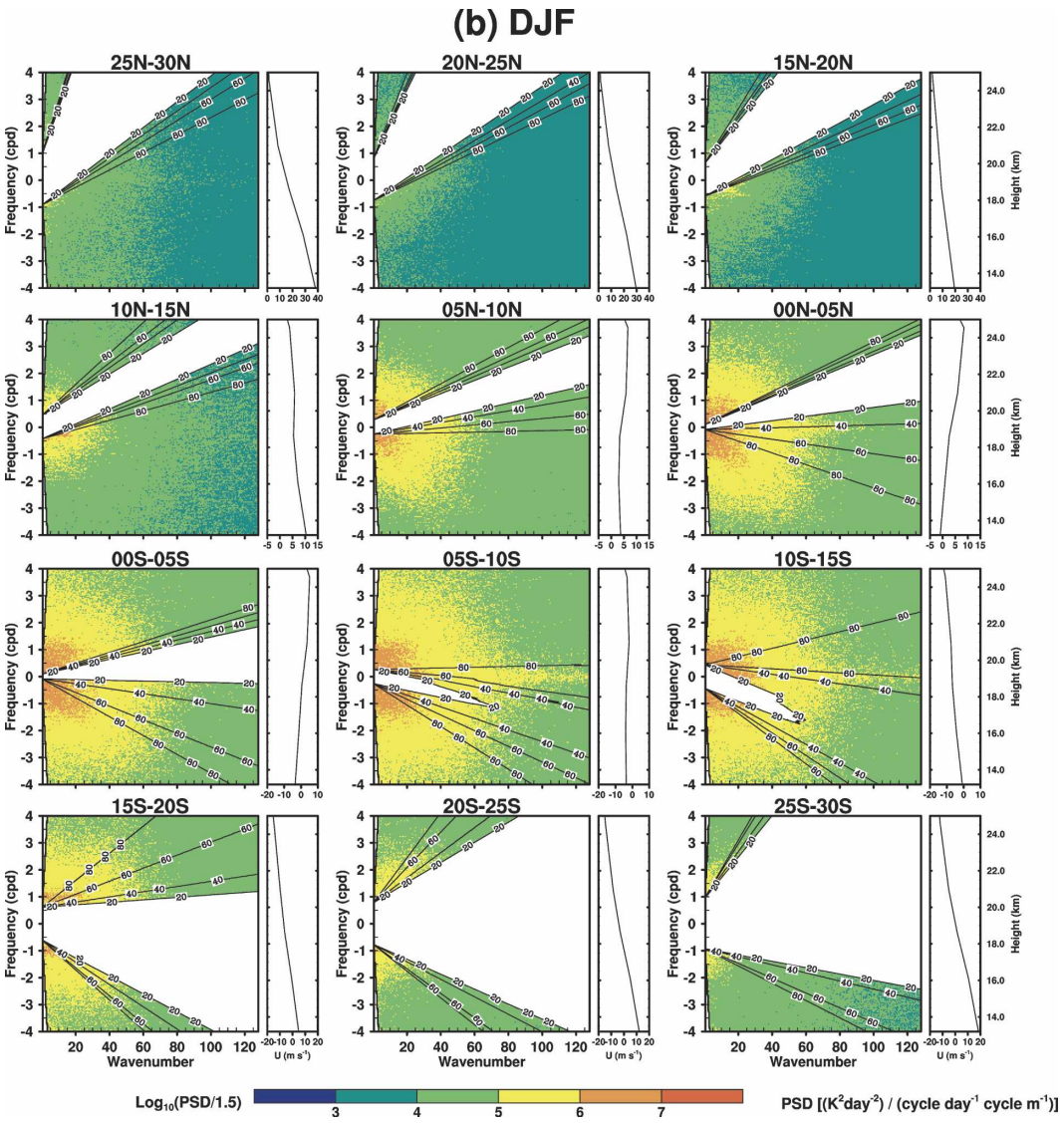

FIG. 9. (*Continued*)

domain shown in Fig. 9 is determined mainly by the zonal-mean zonal wind based on (7)–(8). Since the zonal-mean zonal wind changes with time, we calculate the percentage (lines with numbers) for which a given spectral domain satisfies the vertical propagation condition of IGWs during the 3-month period. There are two lines corresponding to each percentage, which are determined by the minimum and maximum values of zonal-mean zonal wind as shown in Fig. 8. Spectral domains above the upper percentage line and below the lower percentage line denote the areas of wave propagation with that percentage during the 3-month period. The white area denotes the spectral domain in which wave propagation allows less than 20% during the 3-month period. The 3-month averaged zonal-mean zonal wind profile in the target height range in each latitude bin is also plotted on the right side.

In JJA (Fig. 9a), relatively strong wind shear exists between 5°N and 5°S, and consequently, a large portion of the convective forcing there cannot be used to generate gravity waves that can propagate into the stratosphere. At the latitudinal bin of 10°–15°N, on the other hand, a larger portion of source spectrum can be used to generate gravity waves due to the weak wind shear. South of 15°S, the relatively strong westerly near z = 13.2 km decreases rapidly with height up to z = 16–18 km, and this filters out most of the positive phase-speed components of the convective forcing (which have a relatively stronger power than the negative phase-speed components, as shown in Fig. 6a). Similarly,

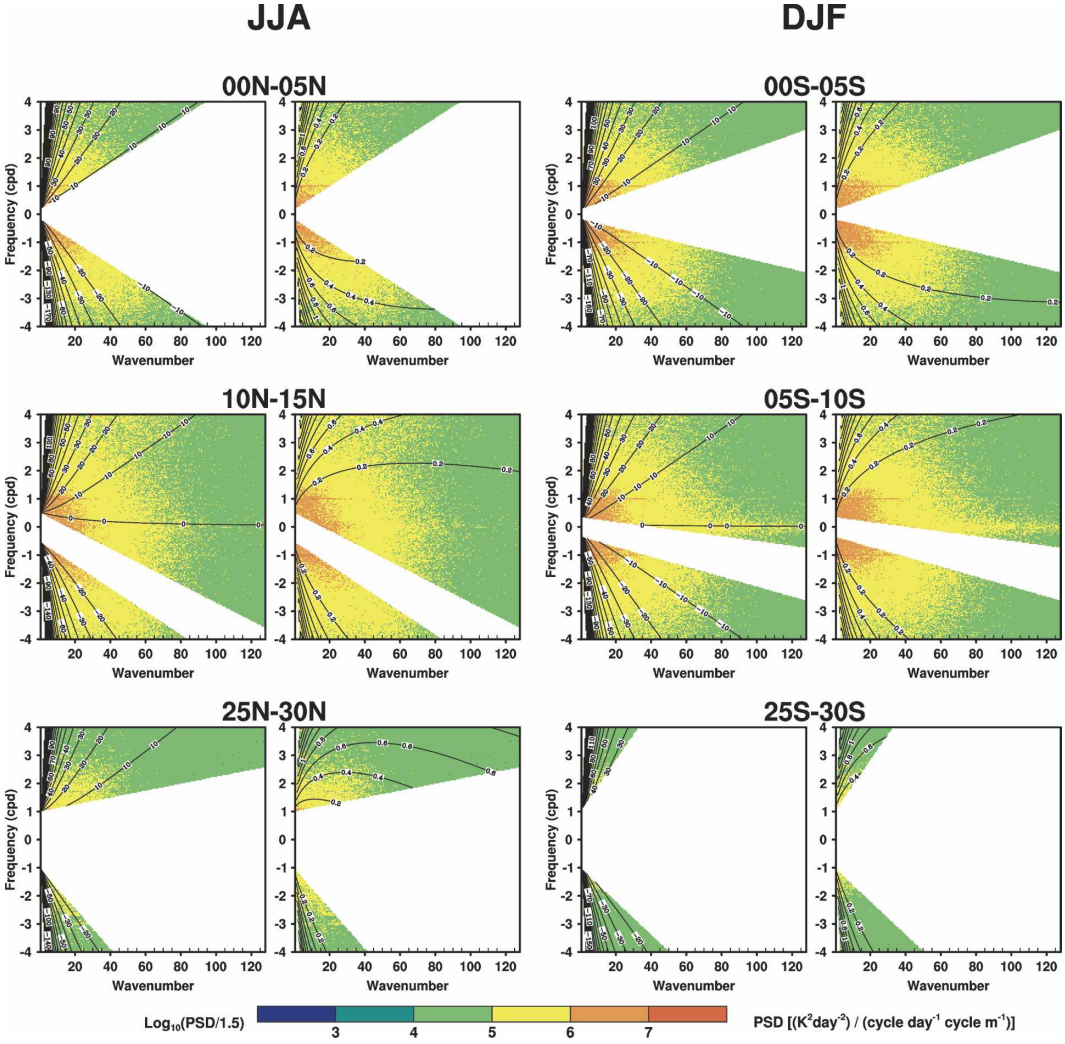

FIG. 10. (left) Zonal and (right) vertical components of group velocity superimposed on the PSD of DCH in selected latitude bins in Fig. 6. The white area denotes wave prohibition ($k_p - \omega_p$ area), which is calculated using the 3-month averaged zonal-mean zonal wind profile in JJA and DJF.

north of 15°N, large portions of the negative phase-speed components of DCH cannot be used to generate gravity waves. In DJF (Fig. 9b), the spectral domains for wave prohibition (white areas) are less in the major forcing region between 10°N and 15°S than in JJA. On the other hand, north of 15°N, large portions of the positive phase-speed components of DCH cannot be used, and south of 20°S, only DCH with very large magnitude of negative and positive phase-speed components can be used to generate stratospheric gravity waves.

In the zonal wavenumber and frequency domain, effective convective sources that allow for vertical propagation of gravity waves in the lower stratosphere correspond to certain horizontal and vertical group velocities, and thus can generate rays of waves that can propagate near or far from the source regions. Figure 10 shows zonal (left panel) and vertical (right panel) components of the ground-based group velocity (black lines with numbers in a unit of meters per second) superimposed on the PSD of DCH in the selected latitude bins shown in Fig. 6. The white area denotes wave prohibition ($k_p - \omega_p$ area), which is calculated using a 3-month mean of the zonal-mean zonal wind at each latitude bin. The zonal and vertical components of the ground-based group velocity can be derived using (3), respectively, as

$$c_{gx} = \frac{\partial \omega}{\partial k} = U + \frac{k(N^2 - \hat{\omega}^2)}{\hat{\omega}(k^2 + l^2 + m^2 + \alpha^2)}, \tag{9}$$

$$c_{gz} = \frac{\partial \omega}{\partial m} = -\frac{m(\hat{\omega}^2 - f^2)}{\hat{\omega}(k^2 + l^2 + m^2 + \alpha^2)}. \tag{10}$$

In the latitude bin of 0°–5°N in JJA and 0°–5°S in DJF, convective sources with a zonal group velocity of less than 10 m s^{-1} and a vertical group velocity of less than 0.2 m s^{-1} are filtered out significantly, especially in JJA. If we assume that a ray of a wave is generated by a convective source at $z = 13$ km and that its horizontal and vertical group velocities are 10 and 0.2 m s^{-1}, respectively, then it takes about 15 h for the wave to reach to 24 km with a longitudinal drift of about 540 km (assuming the group velocities are constant following the ray). Given that the magnitudes of horizontal and vertical group velocities shown in the effective source region in Fig. 10 are larger than those we assumed above, it takes less than 15 h for waves to reach the stratosphere but the zonal drift will be similar by stronger zonal group velocity. In the latitude bins of 10°–15°N in JJA and 5°–10°S in DJF, relatively larger portions of spectral components of DCH can generate gravity waves with very small vertical and horizontal components of group velocity. Therefore, waves generated by convective sources in those latitude bins will propagate mainly in the vertical direction without significant zonal drift, and it will take longer time for waves to reach the stratosphere from the source region. This implies that in the lower stratosphere there is a greater probability to observe waves generated by convective sources in 10°–15°N (5°–10°S) latitudes bin than in the 0°–5°N (0°–5°S) latitudes bin in JJA (DJF). In the higher latitudes bins (25°–30°N in JJA and 25°–30°S in DJF), only convective sources with large positive and negative group velocities are effective, especially in DJF, although their contribution to the stratospheric gravity waves and resultant momentum flux is not likely significant due to their small forcing magnitude.

The results shown in Figs. 9 and 10 demonstrate that the low-frequency components of the convective source can be filtered out significantly even in the lower latitudes depending on the basic-state wind structure, and consequently, that the ground-based vertical group velocity of IGWs generated by the convective source in the lower latitudes is not always smaller than in the higher latitudes. That is, there is no simple relationship between the ground-based vertical group velocity and latitude, and low latitudes are not always favorable for IGWs to be observed in the stratosphere. This implies that the conclusion by Alexander et al. (2002) based on intrinsic frequency arguments without considering latitudinal variations of basic-state wind and convective source may need some modifications.

4. Summary and conclusions

Latitudinal variations of convective sources and propagation condition of inertio-gravity waves were examined using the GCI data with high temporal (3 hourly) and spatial (0.35° latitude × 0.7° longitude) resolutions in the tropical region between 30°S and 30°N during a 1-yr period (March 1985–February 1986) and the 6-hourly NCEP–NCAR reanalysis data, respectively. The convective source was derived by calculating a deep convective heating (DCH) rate that was estimated using the brightness temperature of the GCI data with a threshold value 240 K to represent "deep" cumulus convection. Since latitudinal variation of convective activity in the tropical region differs significantly by season, according to the location of ITCZ, most analyses are carried out separately in JJA and DJF periods.

Latitudinal variation of the convective source in the tropical region is found to be significant throughout the year, and sharp changes of DCH within just a 5° latitude range is observed for most latitudes, especially in the major convective regions (0°–20°N in JJA and 0°–20°S in DJF). To gain a quantitative understanding of convective sources in the tropical region, spectral analyses of the frequency (ω), zonal wavenumber (k), and zonal phase speed (c) were carried out. It was found that on a global scale in the Tropics DCH has a dominant period of 1 day and a zonal wavelength of about 1600 km. The phase-speed spectrum of DCH is Gaussian type and its power decreases rapidly as phase speed increases from the maximal value at $c = 0$. This convective source spectrum is similar to that proposed by Beres et al. (2004) and SC05 for the cloud-top momentum flux formulations of convective GWD parameterizations. Two-dimensional ($k - \omega$) spectra of the convective source calculated for each 5° latitude bin revealed significant latitudinal variations in magnitude, moving direction, and spectral characteristics.

The vertical propagation condition of IGWs is determined, in the zonal wavenumber–frequency domain, by two factors: (i) latitude, which determines the Coriolis parameter, and (ii) the basic-state wind structure in the target height range of wave propagation. Using the 6-hourly NCEP–NCAR reanalysis data, the vertical propagation condition of inertio-gravity waves was calculated from 150 to 30 hPa and superimposed on the two-dimensional ($k - \omega$) spectrum of the convective source in each 5° latitude bin. It was found that the basic-state wind significantly influences the wave propagation condition, and accordingly a large portion of source spectrum is filtered out. This is prominent not only in the latitudes higher than 15° where strong negative shear exists, but also near the equator where strong positive shear associated with the westerly phase of QBO filters out large portions of the low-frequency components of the convective source. The magnitude

of the convective source and its effectiveness in generating gravity waves in the stratosphere are largest in the latitude bins of 10°–15°N in JJA and 5°–10°S in DJF, rather than near the equator. That is, there is no simple relationship between the ground-based frequency (and vertical component of group velocity) and latitude, and low latitudes are not always favorable for IGWs to be observed in the stratosphere. Overall, the characteristics of gravity waves and their latitudinal variations can be understood through the spectral combination of the wave source and the wave propagation condition relative to the ground, and the basic-state wind in the tropical region, which has seasonal, annual, and interannual (e.g., QBO) variations that play a major role not only in determining the wave propagation condition in the stratosphere but also in producing convective source in the troposphere.

Acknowledgments. The authors are grateful to Dr. Murry Salby for providing the original GCI data. The authors thank two anonymous reviewers for their constructive comments. This work was supported by the Korea Research Foundation Grant funded by the Korean Government (MOEHRD) (R02-2004-000-10027-02) and by the Ministry of Science and Technology of Korea through the National Research Laboratory Program.

REFERENCES

Alexander, M. J., T. Tsuda, and R. A. Vincent, 2002: Latitudinal variations observed in gravity waves with short vertical wavelengths. *J. Atmos. Sci.,* **59,** 1394–1404.

Allen, S. J., and R. A. Vincent, 1995: Gravity wave activity in the lower atmosphere: Seasonal and latitudinal variations. *J. Geophys. Res.,* **100,** 1327–1350.

Beres, J. H., 2004: Gravity wave generation by a three-dimensional thermal forcing. *J. Atmos. Sci.,* **61,** 1805–1815.

——, M. J. Alexander, and J. R. Holton, 2004: A method of specifying the gravity wave spectrum above convection based on latent heating properties and background wind. *J. Atmos. Sci.,* **61,** 324–337.

Bergman, J. W., and M. L. Salby, 1994: Equatorial wave activity derived from fluctuations in observed convection. *J. Atmos. Sci.,* **51,** 3791–3806.

Bühler, O., 2003: Equatorward propagation of inertia–gravity waves due to steady and intermittent wave sources. *J. Atmos. Sci.,* **60,** 1410–1419.

Chun, H.-Y., I.-S. Song, J.-J. Baik, and Y.-J. Kim, 2004: Impact of a convectively forced gravity wave drag parameterization in NCAR CCM3. *J. Climate,* **17,** 3530–3547.

Eckermann, S. D., I. Hirota, and W. K. Hocking, 1995: Gravity wave and equatorial wave morphology of the stratosphere derived from long-term rocket soundings. *Quart. J. Roy. Meteor. Soc.,* **121,** 149–186.

Ern, M., P. Preusse, M. J. Alexander, and C. D. Warner, 2004: Absolute values of gravity wave momentum flux derived from satellite data. *J. Geophys. Res.,* **109,** D20103, doi:10.1029/2004JD004752.

Fetzer, E. J., and J. C. Gille, 1994: Gravity wave variance in LIMS temperatures. Part I: Variability and comparison with background winds. *J. Atmos. Sci.,* **51,** 2461–2483.

Janowiak, J. E., and P. A. Arkin, 1991: Rainfall variations in the tropics during 1986–1989 as estimated from observations of cloud-top temperature. *J. Geophys. Res.,* **96,** 3359–3373.

Jiang, J. H., B. Wang, K. Goya, K. Hocks, S. D. Eckermann, J. Ma, D. L. Wu, and W. G. Read, 2004: Geographical distribution and interseasonal variability of tropical deep convection: UARS MLS observations and analyses. *J. Geophys. Res.,* **109,** D03111, doi:10.1029/2003JD003756.

Kalnay, E., and Coauthors, 1996: The NCEP/NCAR 40-Year Reanalysis Project. *Bull. Amer. Meteor. Soc.,* **77,** 437–471.

Karoly, D. J., G. L. Roff, and M. J. Reeder, 1996: Gravity wave activity associated with tropical convection detected in TOGA COARE sounding data. *Geophys. Res. Lett.,* **23,** 261–264.

Marks, C. J., and S. D. Eckermann, 1995: A three-dimensional nonhydrostatic ray-tracing model for gravity waves: Formulation and preliminary results for the middle atmosphere. *J. Atmos. Sci.,* **52,** 1959–1984.

McLandress, C., M. J. Alexander, and D. L. Wu, 2000: Microwave Limb Sounder observations of gravity waves in the stratosphere: A climatology and interpretation. *J. Geophys. Res.,* **105,** 11 947–11 968.

Ricciardulli, L., and R. R. Garcia, 2000: The excitation of equatorial waves by deep convection in the NCAR Community Climate Model (CCM3). *J. Atmos. Sci.,* **57,** 3461–3487.

——, and P. D. Sardeshmukh, 2002: Local time- and space scales of organized tropical deep convection. *J. Climate,* **15,** 2775–2790.

Salby, M. L., H. H. Hendon, K. Woodberry, and K. H. Tanaka, 1991: Analysis of global cloud imagery from multiple satellites. *Bull. Amer. Meteor. Soc.,* **72,** 467–480.

——, F. Sassi, P. Callaghan, W. Read, and H. Pumphrey, 2003: Fluctuations of cloud, humidity, and thermal structure near the tropical tropopause. *J. Climate,* **16,** 3428–3446.

Song, I.-S., 2005: Convectively forced internal gravity waves and their parameterization in large-scale models. Ph.D. dissertation, Yonsei University, 217 pp.

——, and H.-Y. Chun, 2005: Momentum flux spectrum of convectively forced internal gravity waves and its application to gravity wave drag parameterization. Part I: Theory. *J. Atmos. Sci.,* **62,** 107–124.

——, ——, and T. P. Lane, 2003: Generation mechanisms of convectively forced internal gravity waves and their propagation to the stratosphere. *J. Atmos. Sci.,* **60,** 1960–1980.

Tanaka, K., K. Woodberry, H. Hendon, and M. Salby, 1991: Assimilation of global cloud imagery from multiple satellites. *J. Atmos. Oceanic Technol.,* **8,** 613–626.

Tsuda, T., M. Nishida, C. Rocken, and R. H. Ware, 2000: A global morphology of gravity wave activity in the stratosphere revealed by the GPS occultation data (GPS/MET). *J. Geophys. Res.,* **105,** 7257–7274.

——, M. V. Ratnam, P. T. May, M. J. Alexander, R. A. Vincent, and A. MacKinnon, 2004: Characteristics of gravity waves with short vertical wavelengths observed with radiosonde and GPS occultation during DAWEX (Darwin Area Wave Experiment). *J. Geophys. Res.,* **109,** D20S03, doi:10.1029/2004JD004946.

Vincent, R. A., and M. J. Alexander, 2000: Gravity-waves in the tropical lower stratosphere: An observational study of seasonal and interannual variability. *J. Geophys. Res.,* **105,** 17 971–17 982.

Wu, D. L., and J. W. Waters, 1996: Gravity-wave-scale temperature fluctuations seen by the UARS MLS. *Geophys. Res. Lett.,* **23,** 3289–3292.